Journal of Hazardous Materials 416 (2021) 125787

Contents lists available at ScienceDirect

Journal of Hazardous Materials

journal homepage: www.elsevier.com/locate/jhazmat

Research Paper

Degradation synergism between sonolysis and photocatalysis for organic pollutants with different hydrophobicity: A perspective of mechanism and application for high mineralization efficiency

Baekha Ryu [a], Kien Tiek Wong [a,*], Choe Earn Choong [a], Jung-Rae Kim [b], Hyunook Kim [c], Sang-Hyoun Kim [d], Byong-Hun Jeon [e], Yeomin Yoon [f], Shane A. Snyder [g,h], Min Jang [a,*]

[a] Department of Environmental Engineering, Kwangwoon University, 20 Kwangwoon-Ro, Nowon-Gu, Seoul 01897, Republic of Korea
[b] School of Chemical and Biomolecular Engineering, Pusan National University, Busan 46241, Republic of Korea
[c] Department of Environmental Engineering, University of Seoul, Seoul 02504, Republic of Korea
[d] Department of Civil and Environmental Engineering, Yonsei University, Seoul 03722, Republic of Korea
[e] Department of Earth Resources and Environmental Engineering, Hanyang University, Seoul 04763, Republic of Korea
[f] Department of Civil and Environmental Engineering, University of South Carolina, 300 Main Street, Columbia, SC 29208, USA
[g] Chemical and Environmental Engineering, University of Arizona, Tucson, AZ 85721, USA
[h] Nanyang Environment & Water Research Institute (NEWRI), Nanyang Technological University, 1 Cleantech Loop, CleanTech One, Singapore 637141, Singapore

ARTICLE INFO

Editor: Dr. T Meiping

Keywords:
Photocatalysis
Electrons
Hydrogen peroxide
Synergistic
Sonolysis

ABSTRACT

Despite extensive studies, the fundamental understanding of synergistic mechanisms between sonolysis and photocatalysis for the abatement of persistent organic pollutants (POPs) remains uncertain. As different phases formed under ultrasound irradiation, hydrophilic POPs, sulfamethoxazole (SMX, K_{ow}: 0.89), predominantly resides in bulk liquid and is ineffectively degraded by sonolysis ($k_{US} = 3.33 \times 10^{-3}$ min^{-1}) since <10% of hydroxyl radicals (·OH) formed at the gas-liquid interface of cavitation is diffused into the bulk, whereas the other fraction rapidly recombines into hydrogen peroxide (H_2O_2). This study provides a proof-of-concept for the mechanism by presenting various analytical results, endorsing the synergistic role of photoexcited electrons in splitting sonolysis-induced H_2O_2 into ·OH, particularly in the bulk phase. In a sonophotocatalytic system, the hydrophobic POPs such as bisphenol A (BPA) and atrazine (ATZ) were mainly degraded in gas-liquid interface indicated by the low synergistic values correlation compared to SMX [i.e., SMX has a higher synergistic factor, f_{syn} (3.26) than BPA (1.30) and ATZ (1.35)]. Also, f_{syn} was found linearly correlated with the contribution factor of photocatalysis to split H_2O_2. Three times of consecutive kinetics using an effluent of municipal (MP) wastewater spiked by POPs presented >98% POPs and >96% total organic carbon (TOC) removal.

1. Introduction

Emerging persistent organic pollutants (POPs) comprised of anthropogenic chemicals originated from agricultural runoff, municipal and industrial discharge are resistant to environmental degradation and notorious for being poorly treated by the existing wastewater treatment plants (Katsoyiannis and Samara, 2005). The fate of POPs in water resources threatens the safety of our daily water consumption and affects the entire ecosystem. Although POPs exist at a very low concentration (ng-μg L^{-1}) (Zuccato et al., 2000; Bao et al., 2012; Stackelberg et al., 2004), their tendency to bioaccumulation maintains a treat in long-term exposure. Advanced oxidation processes (AOPs) are currently considered one of the most promising approaches for removing POPs. Among AOPs, photocatalysis has been widely studied owing to its promising green route to degrade organic pollutants to harmless end products (Colmenares and Luque, 2014; Babu et al., 2015; Eshaq et al., 2020). Its advantage is the utilization of renewable sources of energy (i.e., sunlight) to activate the semiconductor to generate reactive oxygen species (ROS) without additional chemicals. Besides, acoustic-based AOP (sonolysis) has also received considerable attention lately as a promising approach (Shende et al., 2019; Naddeo et al., 2010; Merouani et al., 2016; Madhavan et al., 2010; Monteagudo et al., 2014) due to the higher amounts of reactive radicals generated during cavities implosion (Brotchie et al., 2009; Yasui et al., 2008).

* Corresponding authors.
E-mail addresses: kientiek@kw.ac.kr (K.T. Wong), minjang@kw.ac.kr, heejaejang@gmail.com (M. Jang).

https://doi.org/10.1016/j.jhazmat.2021.125787
Received 13 January 2021; Received in revised form 23 March 2021; Accepted 27 March 2021
Available online 2 April 2021

The combination between photocatalytic and sonolytic systems was shown to have high capabilities to degrade a wide range of POPs, i.e., dyes (Sancheti et al., 2018; Nuengmatcha et al., 2016; Selim et al., 2020; Mehrizad et al., 2019), pharmaceutical and personal care products (Savun-Hekimoğlu and Ince, 2019, 2017; Fadzeelah et al., 2019; Lee et al., 2018), and agricultural chemicals (Ayare and Gogate, 2020; Mosleh and Rahimi, 2017; Tabasideh et al., 2017). This fact is most likely owing to the synergistic effect between these two systems where the degradation efficiency of sonophotocatalysis is greater than the summated efficiency of both sonolysis and photocatalysis. Although much effort has been devoted to this field, the underlying understanding of the sono-photochemical mechanism on the synergistic effect remains uncertain. Most studies (Supporting Information, Section S1, and Table S1) have mainly interpreted that the synergistic effect of sonophotocatalysis is attributed to the physical factors induced by ultrasound (US) irradiation. Of most-reported synergistic mechanism, de-agglomeration of photocatalyst by US irradiation has been widely considered the primary mechanism responsible for enhanced degradation efficiency (Anju et al., 2012; Saien et al., 2010; Ahmedchekkat et al., 2011; Peller et al., 2003; Torres et al., 2008). The induced US wave was also reported to play an essential role in improving mass transfer between POP(s) and photocatalyst, providing a higher probability of surface reaction (Michael et al., 2014; Hapeshi et al., 2013). The studies conducted by (Gole et al., 2017) and (Zargazi and Entezari, 2019) have addressed that the higher degradation of organic pollutants is attributed to the increase of hydroxyl radicals (·OH) generation in the sonophotocatalytic system. However, in their studies, the mechanism on the superior ·OH generation in sonophotocatalysis compared to a single system was not thoroughly discussed and only generally ascribed to the synergistic effect between sonolysis and photocatalysis. We assumed that these interpretations primarily stem from a limited study towards the chemical reaction without further understanding radicals' dynamic formation in three different phases: gas cavity, gas-liquid interface, and bulk liquid (Merouani et al., 2016; Adewuyi, 2001). Therefore, an in-depth understanding is necessary not only to correlate the synergistic mechanism occurred under the cavitation environment and photocatalytic activities, but also to associate the degradation efficiencies of the POPs with intrinsic physicochemical characteristics, such as hydrophobicity (K_{ow}), distribution coefficient (log D), and acid dissociation constant (K_a).

In this context, the following objectives were set to elucidate the sono-photochemical mechanism via (1) understanding the variation in degradation efficiencies with different physicochemical characteristics of POPs under various AOP systems, (2) determining the contribution of ROS in sonophotocatalysis, and clarifying the transfer pathway of photoexcited charge carriers, (3) comparing the relationship between molecular/surface charges of POPs and TiO_2 against hydrophobicity at different pH, (4) comprehensive assessment on how the phases created within the US environment contribute to synergism, and finally (5) determining the degradation efficiency of POPs in actual municipal (MP) wastewater by sonophotocatalysis and implication on the proposed mechanism. To fulfill the above objectives, three representative POPs, namely, bisphenol A (BPA: plastic monomer), atrazine (ATZ: herbicide), and sulfamethoxazole (SMX: antibiotic, pharmaceutical) were selected based on their distinct physicochemical properties and environmental impact (Table S2). Both BPA and ATZ were classified by the U.S. Environmental Protection Agency (EPA) as endocrine-disrupting compounds (Singh et al., 2018; Goeury et al., 2019; Jagne et al., 2016) that interfere with hormonal systems and induce tumor growth. While SMX does not have a direct impact on the environment, the occurrence of low concentration of antibiotics in water bodies has been reported to promote antibiotic resistance in bacteria (Hoa et al., 2011).

Based on this study, a conceptualized sono-photochemical mechanism was proposed to highlight the crucial role of the photoexcited electron (e^-), which has high selectivity to split US induced hydrogen peroxide (H_2O_2) into a highly reactive ·OH (suitable for degrading a broad spectrum of POPs), instead of converting dissolved O_2 into a less efficient oxidation species, superoxide radicals ($\cdot O_2^-$, unable to degrade negatively charged POPs, i.e., ATZ). This study was performed in three consecutive parts, first section was composed of optimization of the US and photocatalyst for various operational parameters; and degradation achieved by the single and synergistic US and photocatalysis conditions at the optimized conditions. The second section is composed of radical trapping and electron spin resonance (ESR) for the qualitative and quantitative analysis of radicals responsible for the degradation of the pollutants. The pH was varied in the synergistic approach for knowing the dominant factor between hydrophobicity and molecular charge. The H_2O_2 consumption and with increased TiO_2 concentration was found to be high which correlated well with high synergism. The third section is composed of application of an optimized synergistic approach for the treatment of municipal wastewater effluent. Economic assessment of the present synergistic approach for energy requirement was calculated finally. Stability was checked by running the experiment for consecutive three cycles.

2. Materials and methods

2.1. Chemicals

As a photocatalyst, TiO_2 (P25) was purchased from Degussa Corporation. BPA, ATZ, and SMX (purity > 99%), used as targeted POPs, were purchased from Sigma–Aldrich Corporation. Reagent-grade oxalic acid, ferric chloride ($FeCl_2{\cdot}4H_2O$), ferrous sulfate ($FeSO_4{\cdot}7H_2O$), phenanthroline, ammonium molybdate ($H_8MoN_2O_4$), tert-butyl butanol (t-BuOH), sodium oxalate ($Na_2C_2O_4$), potassium dichromate ($K_2Cr_2O_7$), 1,4-benzoquinone (BQ), potassium biphthalate ($C_8H_5KO_4$), sodium hydroxide (NaOH), and potassium iodide (KI) were purchased from Daejung Chemicals. For high-performance liquid chromatography (HPLC) analysis, HPLC grade mobile phase solvent, acetonitrile (ACN, purity> 99.9%) from Daejung Group, as well as Milli-Q ultrapure water were used.

2.2. Experimental setup

The solution temperature was maintained at 25 ± 1 °C using a water circulation chiller (HS-28A, 22–240 V, 50 Hz, HAILEA) and a circulation pump (HX 6530, 50 W, 200–240 V, HAILEA). Mechanical stirring was performed using an overhead stirrer (RZR - 2102 control, Heidolph Instrument) at a constant speed. Two ultraviolet (UVA; wavelength, 350 nm) lights (4 W each, Philips) were used as light sources in the reactor. The reaction tank comprised a customized design dual stainless-steel wall (Φ 110 mm × 170 mm, total volume: 1.5 L with an effective volume of 1 L) with mounting plates and water circulation in/out fittings. The US unit comprised a fabricated stainless-steel transducer module (Fulltech, Taiwan), coupled with an adjustable US power (E_{max}: 100 W) and frequency (Flexonic Mirae Ultrasonic Tech., model FX-4FREQ, Korea). The sonophotocatalytic system is illustrated in Fig. S1.

The actual energy flux incident from the UVA lamp and the US energy dissipation were calculated as described in Section S2. A detailed methodology was described for the photon flux and energy dissipation, characterization of TiO_2, experimental setup, and other relevant information are described in Section S2.1–S2.7. The optimization for temperatures, US powers, and US frequencies for sonophotocatalytic degradation and spectroscopic analyses for TiO_2 were listed in Section S3 and S4, respectively. The figures related to these analyses were depicted in Figs. S2–S10.

3. Results and discussion

3.1. Synergism between sonolysis and photocatalysis

Theoretically, upon US irradiation, the rapid changes of pressure in the water at periodic compression and expansion result in the formation and growth of vapor-filled cavities, known as microbubbles (Pokhrel et al., 2016). These microbubbles are an important factor in creating three phases: gas cavity, gas-liquid interface, and bulk liquid (Adewuyi, 2001). At a certain point, the microbubbles collapse adiabatically in a short time and generate high pressure (~1000 atm) and temperature (~5000 K) within the gaseous region, known as localized hotspot (Xu et al., 2013). This condition provides sufficient energy for splitting water molecules, particularly within the gas-liquid interface, forming a predominant local concentration of highly reactive·OH and hydrogen radicals (·H) (Ajo et al., 2017; Joseph et al., 2009). The sonolytic degradation of three selected POPs at an optimized frequency (35 kHz) was performed to validate the significance of these phenomena, as illustrated in Fig. 1(a) (the frequency optimization was predetermined, as shown in Section S3 and Fig. S6). The degradation rate constants, k_1 (min^{-1}), decreased in the following order: BPA (3.0×10^{-2}) >ATZ (1.6×10^{-2}) > SMX (3.0×10^{-3}). In general, two main properties of POPs dictate the sonolytic degradation: Henry's law constant and hydrophobicity (K_{ow}) (Table S2) (Wu and Ondruschka, 2005). As non-volatile organic compounds, these selected POPs are not expected to partition significantly into the microbubbles' gaseous phase; hence, sonolytic thermal destruction was not considered. POPs with high K_{ow} (i.e., BPA: 3.32 and ATZ: 2.61) have higher affinities at the gas-liquid interface (Jun et al., 2019; Henglein and Gutierrez, 1988), the degradation rate constants for both BPA and ATZ were 9.2 and 4.9 times higher than that of SMX. This result can be explained by the fact that the predominant·OH occurs at the gas-liquid interface and only <10% diffuses into the bulk solution, becoming H_2O_2 (Dharmarathne et al., 2013; Wood et al., 2017; Henglein, 1995). The lowest degradation rate constant for SMX was justified by its hydrophilic nature (K_{ow}: 0.89) since SMX is mostly allocated within the bulk liquid (Mullick and Neogi, 2017; Soltani et al., 2016). Other factor that influences the degradation of BPA, ATZ and SMX were discussed in the pH section. Based on this information, it was postulated that different phases are formed under US irradiation and that the K_{ow} values of the POPs have a significant impact on the degradation activities. The sonolytic degradation of POPs shown in Fig. 1(b) illustrates the cavitational implosion of microbubbles and emphasizes POPs and ROS's existence in the different phases. Contrary to the sonolytic degradation, the order of the photocatalytic degradation rate constants [Fig. 1(c)] did not follow the degree of K_{ow} of the POPs, i.e., ATZ >BPA >SMX with 4.80×10^{-2}, 3.68×10^{-2}, and 1.62×10^{-2} min^{-1}, respectively. As only one phase (bulk solution) existed, the degradation phenomena of the POPs did not depend on the intrinsic K_{ow}

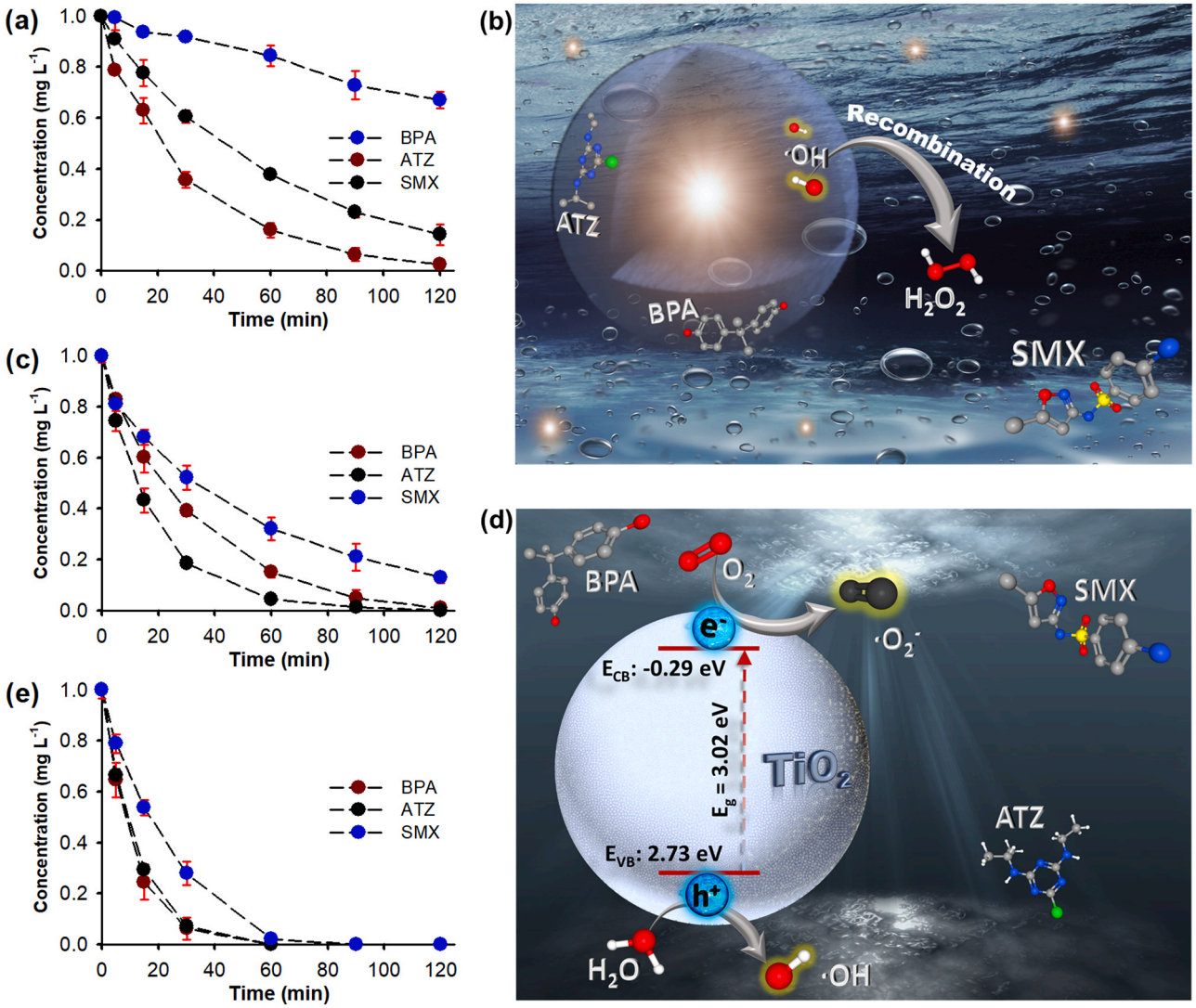

Fig. 1. Degradation kinetics of three POPs by (a) US, (c) UVA/TiO_2 and (e) US/UVA/TiO_2. The schematic mechanisms were depicted for (b) US and (d) UVA/TiO_2.

values. Instead, the pK_a values of the POPs and the surface charge of TiO_2 were primary factors affecting the degradation (Gupta and Modak, 2020; Wong et al., 2020). Based on the photo-optical analysis and PEC analyses, the E_{CB} and E_{VB} of TiO_2 were found to be −0.093 eV and +2.93 eV, respectively. With this electronic structure, TiO_2 was expected to be able to produce $\cdot O_2^-$ and ·OH from the CB and VB, respectively, since the band potentials are higher than the redox potentials of $O_2/\cdot O_2^-$ and $H_2O/\cdot OH$, which are −0.046 and +2.93 V vs. NHE, respectively (Zhou et al., 2014). Hence, Fig. 1(d) highlights that the photo-generated reactive species (h^+,·OH, and$\cdot O_2^-$) exist in the same phase as the three POPs.

Based on the theory described above, we investigated the synergism between sonolytic and photocatalytic degradation for each POP in terms of the synergistic factor, f_{syn}, defined as follows (Eq. 1):

$$f_{syn} = \frac{k_{US/UVA/TiO_2}}{k_{US} + k_{UVA/TiO_2}} \quad (1)$$

Where k_{US}, $k_{UVA/TiO2}$, and $k_{US/UVA/TiO2}$ refer to kinetic rate constants of sonolytic, photocatalytic, and sonophotocatalytic degradations, respectively. The kinetics of the sonophotocatalytic degradation and the f_{syn} for each POP is shown in Fig. 1**(e)** and Table S4, respectively. The decreasing order of the kinetic rate constants by sonophotocatalysis for

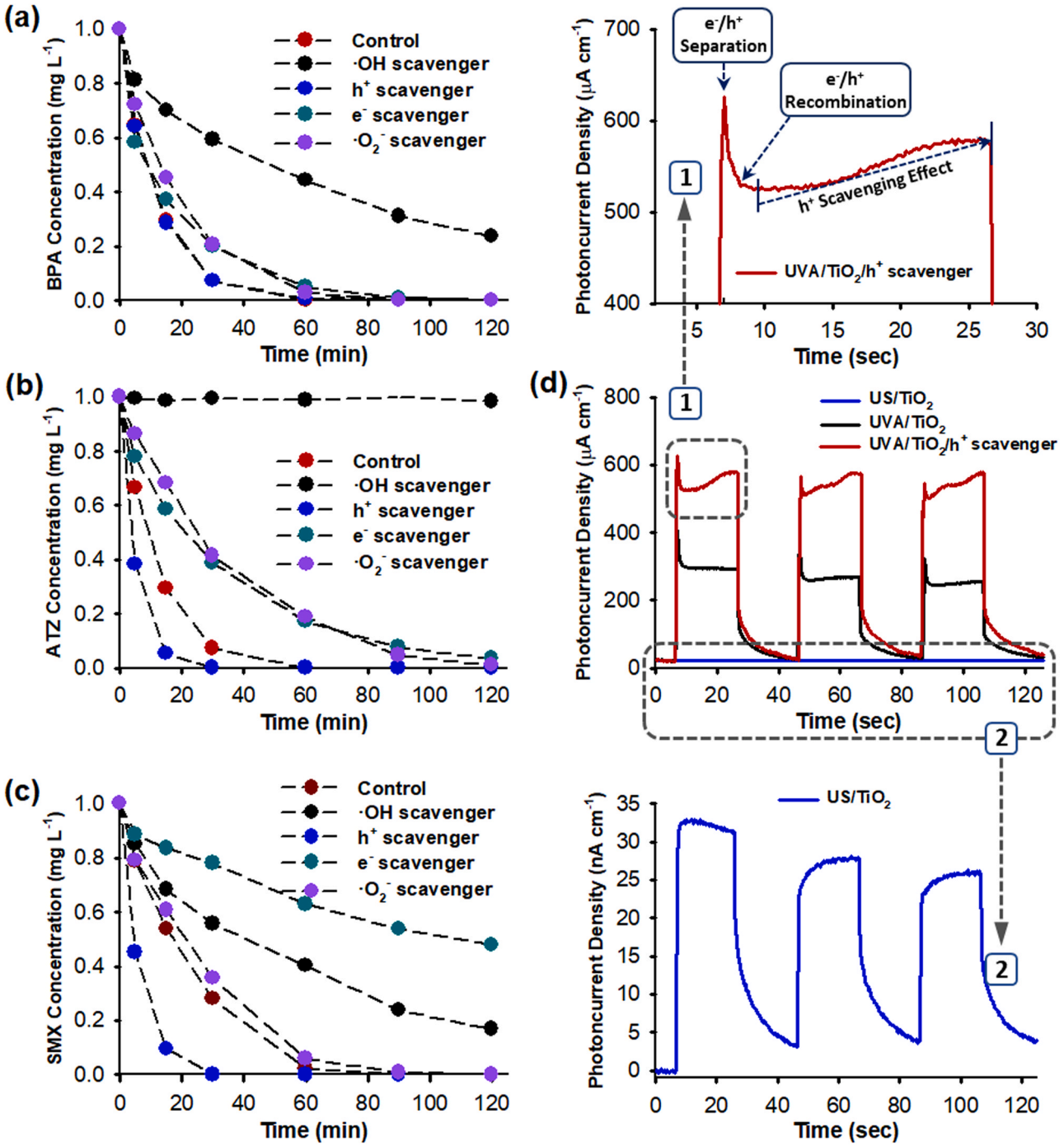

Fig. 2. Effect of radical scavengers on sonophotocatalysis (US/UVA/TiO_2) for (a) BPA, (b) ATZ, and (c) SMX. (d) Photocurrent density measurement under different conditions with enlargement of area indicated by 1 and 2: (1) h^+ scavenging effect and (2) TiO_2 activation by sonoluminescence (US). (t-BuOH: 0.2 mM, $Na_2C_2O_4$: 0.2 mM, $K_2Cr_2O_7$: 20 μM and BQ: 20 μM were used to scavenge ·OH, h^+, e^- and $\cdot O_2^-$, respectively).

POPs was BPA > ATZ >SMX with 8.75×10^{-2}, 8.67×10^{-2}, and 6.37×10^{-2} min^{-1}, respectively. Among the three POPs, the highest f_{syn} was 3.26 for SMX, followed by 1.35 and 1.30 for ATZ and BPA, respectively. The relative contribution ratio (R_{US}) of sonolysis to sonophotocatalysis ($k_{US}/k_{US/UVA/TiO2}$) demonstrates a direct correlation with the intrinsic K_{ow} (BPA > ATZ > SMX). This trend suggests that the R_{US} (Table S4) was inversely related to f_{syn}, where f_{syn} was enhanced with less contribution of ultrasonic irradiation and more involvement with photocatalytic activity.

3.2. Construction of a conceptualized mechanism

To gain insight into the contribution of involving ROS in sonophotocatalysis, scavenging tests for·OH,·O_2^-, h^+, and e^- were conducted [Fig. 2(a)–(c)]. The kinetic rate constants for each scavenging test are shown in Table S5, where k_{scav} and $k_{US/UVA/TiO2}$ denote the kinetic rate constants obtained from each scavenging test and the control experiment, respectively. In terms of the kinetic rate constants (Fig. S11), a similar scavenging trend was observed for BPA and ATZ in the decreasing order of photoexcited species (·OH > e^- > ·O_2^- > control > h^+), whereas SMX showed a different sequence (e^- > ·OH > ·O_2^- > control > h^+). The absence of·OH decreased the kinetic rate constants for BPA and ATZ by 86.9% (1.14×10^{-2} min^{-1}) and 99.9% (1.18×10^{-5} min^{-1}), respectively, proving that·OH was the dominant ROS owing to its non-selective and high oxidation potential (+2.8 V vs. NHE) (Khataee and Fathinia, 2013). It is noteworthy that ATZ was not degraded in the absence of·OH owing to the electrostatic repulsion between anionic ·O_2^- and negatively charged ATZ which hinders the reaction between them (Granados-Oliveros et al., 2009). Interestingly, the kinetic rate constant of SMX reduced significantly by the addition of an e^- scavenger (5.97×10^{-3} min^{-1}, 90.6% reduction) instead of the·OH scavenger (1.18×10^{-2} min^{-1}, 81.4% reduction), whereas the absence of e^- decreased the kinetic rate constants of BPA and ATZ by 45.3% (4.78×10^{-2} min^{-1}) and 68.2% (2.76×10^{-2} min^{-1}), respectively. Hence, the role of e^- for degrading BPA and ATZ was not as important as that for SMX. Contrary to the expected inhibition effect of scavengers, the presence of the h^+ scavenger demonstrated a significant enhancement in the kinetic rate constants particularly for SMX and ATZ, i.e., improvements of 143.3% and 124.9%, respectively.

The oxidation of oxalate by h^+ produces carbon dioxide anion radicals ($CO_2^{\cdot-}$). Because of its strong reducing potential (E°: $CO_2/CO_2^{\cdot-}$ = −1.9 V vs. NHE), $CO_2^{\cdot-}$ can inject e^- into the CB of TiO_2 [(R1)–(R2)] (Jinhua Ye et al., 2016), thus prompting the elevation of photoexcited e^- on TiO_2.

$$HCO_2^- + h^+ \rightarrow CO_2^{\cdot-} + H^+ \quad \text{(R1)}$$

$$CO_2^{\cdot-} \rightarrow CO_2 + e_{CB}^- \quad \text{(R2)}$$

The results of photocurrent density measurements shown in Fig. 2(d) suggest that the photocurrent densities (average of 500 and 550 μA cm^{-2}) were enhanced by nearly 100% in the presence of the h^+ scavenger, yielding discernible peaks in comparison with TiO_2/UVA (average of 250 μA cm^{-2}). Fig. 2 labeled as (Katsoyiannis and Samara, 2005) in Fig. 2(d) indicates three stages of the e^- transfer mechanism: (i) separation, (ii) recombination of carriers, and (iii) h^+ scavenging effect. The increment in photocurrent at stage (iii) is indicative of e^- injection from $CO_2^{\cdot-}$ on TiO_2 (Liu et al., 2013). However, for the removal of BPA, the h^+ scavenger did not increase the kinetic rate constant (8.83×10^{-2} min^{-1}) compared to the control (8.75×10^{-2} min^{-1}). As discussed in Section 3.1, the BPA degradation occurred primarily at the microbubbles' gas-liquid interface, whereas the photoexcited e^- primarily resided in bulk.

Based on the data, we herein propose a hypothesis that the photoexcited e^- is fundamental for the sonophotocatalytic degradation of hydrophilic organic pollutants but minimally affects the hydrophobic compounds. A conceptualized mechanism was designed based on kinetics and various analyses to construct the role of photoexcited e^- in sonophotocatalysis. As outlined in the kinetics above, hydrophilic POPs are less likely to react with·OH owing to their fast recombination in forming H_2O_2. To confirm this hypothesis, the concentration of H_2O_2 formed by each AOP was measured via KI dosimetry (Kormann et al., 1988). Only US irradiation [Fig. 3(a)] exhibited a linear accumulation of H_2O_2 at the rate of 5.5×10^{-2} mmol L^{-1} h^{-1}. The accumulation of H_2O_2 was attributed to the non-addition of POPs; consequently,·OH species recombine rapidly to form H_2O_2 (Torres et al., 2008) based on (R3) and (R4),

$$H_2O \overset{US}{\rightarrow} \cdot OH + \cdot H \quad \text{(R3)}$$

$$\cdot OH + \cdot OH \rightarrow H_2O_2 \left(k_{\cdot OH/\cdot OH} = 5.5 \times 10^9 M^{-1} s^{-1}\right) \quad \text{(R4)}$$

In the presence of POPs, the obtained yield of H_2O_2 under sonolysis decreased in the order of SMX <ATZ < BPA [Fig. 3(a)]. From these results, the consumption of·OH in the degradation activities was calculated as follows (Eq. 2):

$$[H_2O_2]_{consumed}(\%) = \frac{[H_2O_2]_{withoutPOPs} - [H_2O_2]_{withPOPs}}{[H_2O_2]_{withoutPOPs}} \times 100\% \quad (2)$$

From (Eq. 2), it was found that 73.5% and 64.5% of produced H_2O_2 (without POP as control) were utilized for BPA and ATZ degradation for 2 h, respectively. However, for SMX degradation, only 33.8% of the produced·OH was consumed. BPA and ATZ consumed 3.4- and 3.2-times higher amounts of·OH, respectively, compared with SMX, supporting the fact that hydrophobic POPs were mainly degraded via the gas-liquid interface.

Meanwhile, without the addition of POPs, the H_2O_2 evolution by US/UVA or US/TiO_2 resulted in a decrease of ~22.2% or 30.0%, respectively, in comparison with the control (US) [Fig. 3(b)]. These outcomes implied that UVA photons could split H_2O_2 via the oxygen-oxygen bond's photolytic decomposition (R5) (Paleologou et al., 2007). Under the US/TiO_2 system, the sonoluminescence (UVB and UVA) (Cui et al., 2017) produced by the microbubble implosion activates TiO_2 to photoexcite e^-, splitting H_2O_2 into·OH (R6).

$$H_2O_{2(US)} \xrightarrow{UVA} \cdot OH + \cdot OH \quad \text{(R5)}$$

$$H_2O_{2\ (US)} + TiO_2 \xrightarrow{e^-/sonoluminescence} \cdot OH + OH^- \quad \text{(R6)}$$

In comparison with the results above (US, US/UVA, US/TiO_2), US/UVA/TiO_2 had the lowest H_2O_2 concentration, postulating the highly enhanced splitting of H_2O_2 [Fig. 3(b) inset]. The concentration of H_2O_2 under sonophotocatalysis increased slightly to ~0.025 mg L^{-1} at 5 min and almost plateaued, demonstrating a 99.3% reduction compared to that under sonolysis (3.76 mg L^{-1}) at 2 h.

Considering the maximum light intensities at UVA (UVA_{max}: 380 nm) and UVB (UVB_{max}: 306 nm) emitted by sonoluminescence, their corresponding energies were calculated to be 3.9×10^{-6} and 1.8×10^{-5} W L^{-1}, respectively (Fig. S12). This result indicates that the number of photons emitted from the UVA lamp (8 W, 1.47×10^{19} photons s^{-1}) was considerably larger than those emitted from sonoluminescence (UVA_{max}: 2.77×10^{13} photons s^{-1} and UVB_{max}: 7.46×10^{12} photons s^{-1}). The labeled (Zuccato et al., 2000) photocurrent density measurements designated in [Fig. 2(d)] indicating the current densities (average of 27 nA cm^{-2}) via sonoluminescence were lower than those under UVA/TiO_2 (average of 200 and 250 μA cm^{-2}) by four orders of magnitude, indicating a reliable discrepancy. Based on (R5) and (R6), the H_2O_2 consumption rates can be obtained through subtracting the H_2O_2 concentrations for each system at 2 h, i.e., those of the UVA photons ($[H_2O_2]_{US} - [H_2O_2]_{US/UVA}$), sonoluminescence photons ($[H_2O_2]_{US/UVA} - [H_2O_2]_{US/TiO2}$), and photoexcited e^- ($[H_2O_2]_{US/UVA} - [H_2O_2]_{US/UVA/TiO2}$) were 0.42, 0.15, and 1.44 mg L^{-1} h^{-1}, respectively. Therefore, the photoexcited e^- served a dominant role in splitting H_2O_2

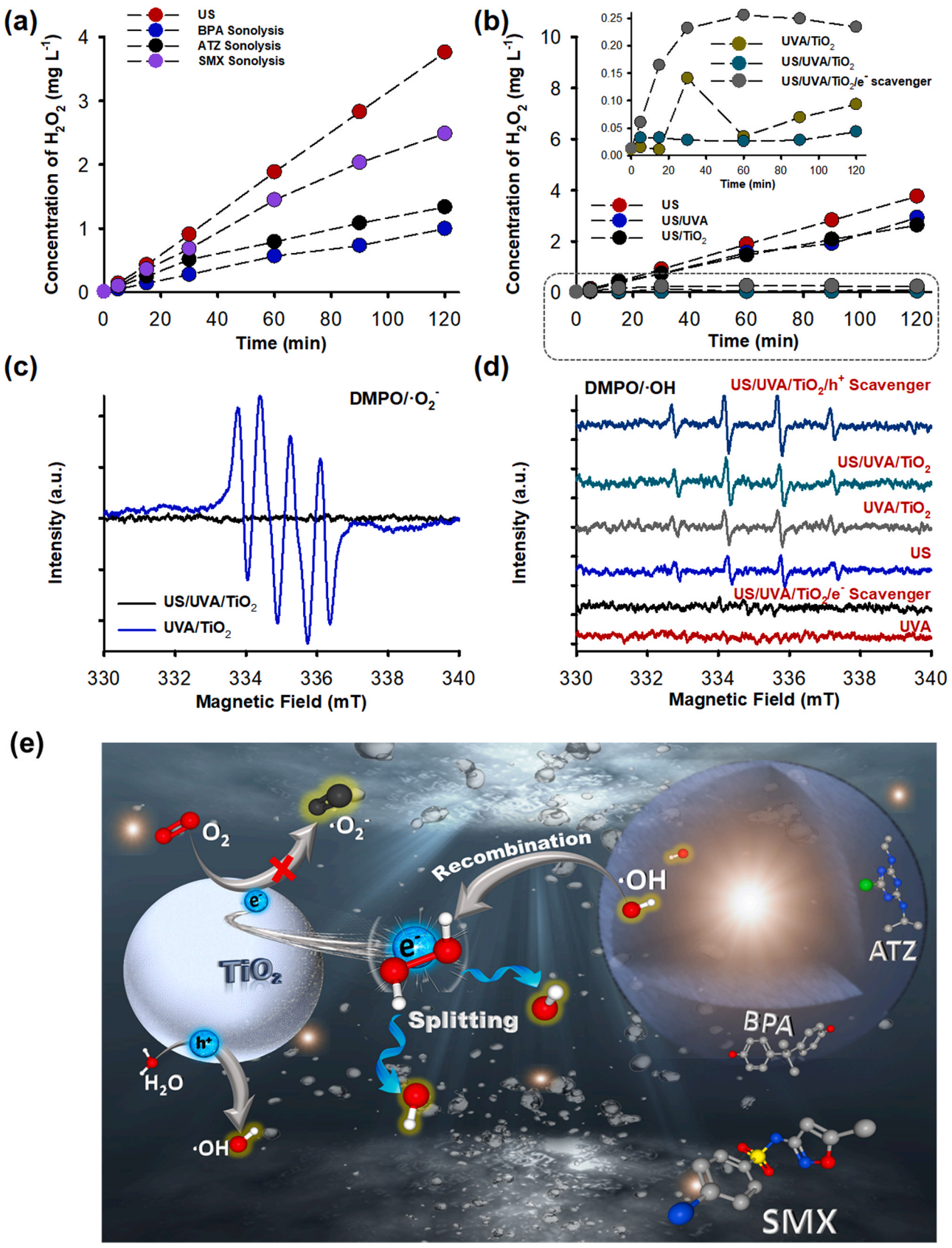

Fig. 3. (a) Kinetics increment of H_2O_2 with and without POPs by KI dosimetry, (b) measurement of H_2O_2 generated by all AOPs in DI water, ESR analysis measurement by DMPO for (c) $\cdot O_2^-$ and (d) ·OH. Inset in (b) indicates the enlargement of H_2O_2 produced. Schematic illustration (e) of the proposed sonophotocatalytic mechanism for the degradation of BPA, ATZ and SMX.

(~0.04 mg L^{-1} at 2 h). As discussed in Section 3.2., accordingly, the highest f_{syn} for SMX could be explained by the fact that the photoexcited e^- generated from TiO_2 upon UVA irradiation stimulates the splitting of H_2O_2 formed by US to produce more·OH in the bulk phase. Since H_2O_2 (+0.39 V vs. SRP) has a higher redox potential than O_2 (−0.18 V vs. SRP) (Mailloux, 2015), it is highly likely that the photoexcited e^- preferentially reacted with H_2O_2 rather than O_2. Therefore, the photoexcited e^- can be preferably utilized to produce higher oxidation potential radicals·OH instead of·O_2^-; this is an essential aspect for the degradation of various POPs. As a piece of supporting evidence to the statement above, the concentration of DO under the sonophotocatalytic degradation of SMX was found to be kinetically constant (~6.5 mg L^{-1}) (Fig. S13). In contrast, those under photocatalysis decreased gradually, indicating that the DO was consumed to form·O_2^- (detailed explanation in Section S5).

The H_2O_2 concentration (0.25 mg L^{-1}) by e^- scavenged sonophotocatalysis at 2 h was higher than that by sonophotocatalysis alone; however, contrary to our expectation, it was much lower than that by US, US/UVA, or US/TiO_2 [inset of Fig. 3(b)]. The low concentration of H_2O_2 can be correlated to the scavenging effect of·OH produced by photoexcited h^+ (ElMetwally et al., 2019), as shown in (R7) and (R8),

$$H_2O_2 \quad _{(US)} + \cdot OH_{(holes/TiO_2)} \rightarrow \quad H_2O + \cdot O_2H \tag{R7}$$

$$\cdot OH_{(holes/TiO_2)} + \quad \cdot O_2H \rightarrow \quad H_2O + O_2 \tag{R8}$$

The reactions shown above prove the important role of photoexcited e^- in splitting the H_2O_2 generated and reducing the self-scavenging effect. The degradation of SMX was further enhanced by the presence of h^+ scavenger, claiming that more photoexcited e^- would split H_2O_2 without the recombination with h^+. Since both the hydrophobic POPs, BPA and ATZ, are preferably degraded by·OH created by microbubble implosion, the role of photoexcited e^- in H_2O_2 splitting is relatively insignificant. This hypothesis justifies the lower f_{syn} values for BPA and ATZ in comparison with that for SMX. To support these results,·O_2^- or·OH was detected via ESR spin trapping using the DMPO abduction method. Under UVA/TiO_2, a typical signal with a 1:1:1:1 intensity ratio of DMPO-·O_2^- indicated the generation of·O_2^- [Fig. 3(c)]. However, this signal was not detected under US/UVA/TiO_2, proving that H_2O_2 predominantly reacts with the photoexcited e^-. Furthermore,·OH abduction was observed with the signal at an intensity ratio of 1:2:2:1. The intensity heights of the detected DMPO-·OH decreased in the following order: US/UVA/TiO_2/h^+ scavenger > US/UVA/TiO_2 > UVA/TiO_2 > US > US/UVA/TiO_2/e^- scavenger [Fig. 3(d)]. Only a small concentration of·OH was produced under sole US irradiation, whereas US/UVA/TiO_2 and UVA/TiO_2 indicated enhanced values of·OH. The·OH signal with the highest intensity was detected with the addition of the h^+ scavenger. The detection of undefined quartet peaks of DMPO-·OH with e^- scavenger implied that the photoexcited e^- served as the primary source for H_2O_2 splitting and its absence triggered the scavenging effect of H_2O_2 by·OH generated from h^+. This correlated well with the effect of e^- scavenger on H_2O_2 concentration, as shown in Fig. 3(b), verifying the consumable reaction between·OH and H_2O_2 in (R7) and (R8). A detailed description of overall redox reactions was listed in Section S6 (Figs. S14–S15) proved that H_2O_2 concentration decreased due to the self-decomposition by ·OH. The ROS reaction pathway is depicted in Fig. S16. As shown in Fig. 2(c), the dramatically impeded SMX degradation by the e^- scavenger highlighted the importance of photoexcited e^- for splitting H_2O_2. Otherwise, both crucial oxidation species (H_2O_2 and·OH) can be self-destructed. The overall synergistic mechanism is illustrated in Fig. 3(e).

3.3. Effects of solution pH on the synergistic mechanism

The influence of the intrinsic hydrophobicity of each POP on the sonophotocatalytic degradation was further investigated by adjusting the solution pH since the electrical charges of the POPs (Fig. S17) and the point of zero charges (pH_{PZC} = ~7) of TiO_2 would affect the degradation of POPs (Cui et al., 2017). The kinetic degradation for each POP is shown in Fig. 4(a)–(c). In general, the f_{syn} values increased in the order of decreasing log D (Table S6). This result is consistent with the previous discussion in Section 3.2, indicating that the hydrophobicity of POPs is the critical factor for the synergistic effect. The distribution coefficient (log D) of each POP was calculated at specific pH values (Gao and Deshusses, 2011) as follows (Eq. 3):

$$LogD = LogK_{ow} - Log\left[1 + 10^{(pH - pK_a)}\right] \tag{3}$$

A higher log D indicates a higher hydrophobicity of the POP. The log D (4.04) for BPA was constant until pH 9, and then it decreased by half at pH 11 [Fig. 4(d)]. By contrast, the log D of ATZ increased with the pH from 3 to 5 and then remained constant at 2.2 until pH 11. SMX exhibited negative log D values at both extreme pH values, suggesting its hydrophilic nature. Both ATZ and SMX had the highest kinetic rate constants, i.e., 0.23 min^{-1} at pH 3 and 0.207 min^{-1} at pH 11, respectively. These results indicate that the electrostatic repulsion or attraction between the POPs and the TiO_2 surface did not play an important role. For instance, at pH 3, most ATZ molecules exist as positively charged (Fig. S17), inducing electrostatic repulsion with the protonated TiO_2 ($TiOH_2^+$). Similarly, electrostatic repulsive forces were present between the negatively charged SMX and deprotonated TiO_2 (TiO^-) at pH 11. Nevertheless, the highest f_{syn} values were calculated for both ATZ and SMX at 3.60 and 10.6, respectively. These outcomes were closely related to the log D values [Fig. 4(d–f), Table S6]; in particular, SMX with a log D of −0.15 (higher affinity to the bulk solution) at pH 11 had the highest f_{syn} (10.6) in comparison with those at pH 7 (f_{syn} = 3.3, log D = 0.20) and pH 3 (f_{syn} = 2.0, Log D = 0.75). Likewise, ATZ had the lowest hydrophobicity at pH 3 (log D = 1.1) and a higher f_{syn} (3.6) than those at pH 7 (1.35) and 11 (0.34). In general, the decrease in log D resulted in enhanced synergism especially the results shown in Fig. 4(e–f). Additionally, other factors might affect the degradation efficiencies of these POPs. At high alkalinity, ·OH generated at the gas-liquid interface self-recombines into H_2O_2 (Ince and Tezcanli-Güyer, 2004; Méndez-Arriaga et al., 2008) and scavenged by the CO_3^{2-} and HCO_3^- (Wang et al., 2009). As CO_2 has a high Henry's constant (3×10^{-3} atm m^3 mol^{-1}), it can typically diffuse into the gaseous phase of the cavitation, resulting in a large fraction of soluble CO_3^{2-}/HCO_3^- at the gas-liquid interface in comparison with the bulk phase. Because of its hydrophilic nature, SMX was primarily distributed in the bulk solution and has minimal effect by these scavengers. ATZ had lower f_{syn} at higher pH, where the generated·OH can be scavenged by CO_3^{2-}/HCO_3^-. However, the highly hydrophobic BPA had an almost constant f_{syn} as a result of less involvement of photoexcited e^- throughout the pH range.

3.4. Correlation between H2O2 consumption and the synergistic factor

In this section, the proposed synergistic mechanism is further elucidated by correlating the relationship between the concentration of H_2O_2 being split under sonophotocatalysis and the synergistic factor (f_{syn}). To begin with, we conducted two sets of kinetics: photocatalysis [Fig. 5(a)] and sonophotocatalysis [Fig. 5(b)] for SMX (the highest f_{syn}) removal with various concentrations of TiO_2. The SMX degradation rate constants for photocatalysis increased gradually from 9.7×10^{-3} to 2.5×10^{-2} min^{-1} as the dosage of TiO_2 increased from 0.01 to 0.1 g L^{-1}; however, they did not show a linear trend under sonophotocatalysis [Fig. 5(c)], in which the lowest kinetic rate constant (1.5×10^{-2} min^{-1}) was obtained at 0.01 g L^{-1} TiO_2 and the highest (6.4×10^{-2} min^{-1}) was obtained at 0.05 g L^{-1}. In contrast to the photocatalysis trend, especially, higher dosages of TiO_2 (>0.05 g L^{-1}) under sonophotocatalysis had lower constants (i.e., 4.5×10^{-2} or 4.2×10^{-2} min^{-1} for 0.07 0.1 g L^{-1} for photocatalysis and sonophotocatalysis, respectively). Based on the obtained constants for the respective photocatalysis and

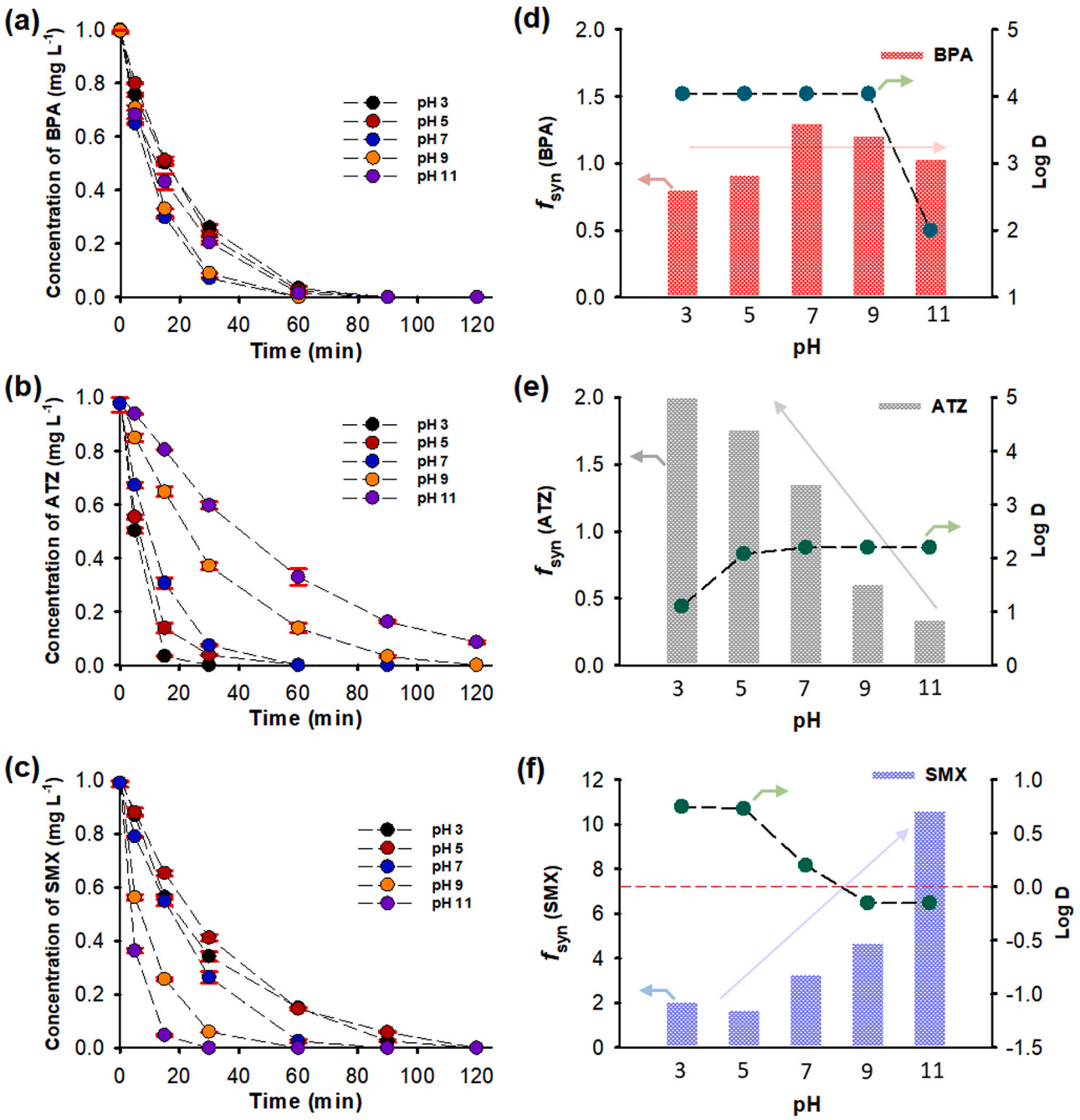

Fig. 4. Initial pH effect on sonophotocatalysis for (a) BPA, (b) ATZ, (c) SMX. The intrinsic property changes of POPs at different pH distribution coefficient (Log D) against synergistic factor for (d) BPA, (e) ATZ, (f) SMX.

sonophotocatalysis, the f_{syn} for each concentration of TiO_2 was calculated, as shown in Fig. 5(c). As discussed in the above sections, the synergistic mechanism is mainly attributed to the sono-photochemical reaction between the photogenerated e^- and H_2O_2 generated by US. Therefore, along with the kinetics, we measured the H_2O_2 concentrations for US/TiO_2 and US/UVA/TiO_2 without SMX [Fig. 5(d)]. Under US irradiation, H_2O_2 generation for 2 h decreased gradually with an increase of TiO_2 dosage (0.01 – 0.1 g L^{-1}) owing to the photoactivation of TiO_2 by sonoluminescence caused by microbubble implosion. Compared with the H_2O_2 generation by US (3.76 mg L^{-1}) for 2 h, TiO_2 addition reduced by 0.8–15.3%. However, in US/UVA/TiO_2, the H_2O_2 concentrations were significantly lower than those for US/TiO_2. This result is attributed to the four-orders-of-magnitude-stronger energy emitted from UVA to generate photoexcited e^- from TiO_2 compared to those from sonoluminescence. With a low concentration of TiO_2 (0.01 g L^{-1}), the limited photoactive surfaces resulted in lower numbers of photoexcited e^-, consequently providing an insufficient splitting of H_2O_2. Compared with US/UVA (2.92 mg L^{-1} for 2 h), 0.01 g L^{-1} of TiO_2 addition split 47.6% of H_2O_2. The splitting of H_2O_2 by 0.03 or 0.05 g L^{-1} of TiO_2 increased significantly to 94.5% or 96.4%, respectively, whereas a higher dose of TiO_2 indicated a decline in H_2O_2 splitting by 69.5% and 62.8% at 0.07 and 0.1 g L^{-1}, respectively.

The highest f_{syn} (3.26) was obtained with 0.05 g L^{-1} of TiO_2. At concentrations higher than 0.05 g L^{-1} of TiO_2, the f_{syn} decreased significantly (i.e., 1.80 and 1.51 for 0.07 and 0.1 g L^{-1}, respectively). The increase in suspension turbidity can justify this phenomenon due to higher dosage followed by the de-agglomeration of TiO_2, which decreases the incident light penetration depth (Rad et al., 2020; Kakavandi

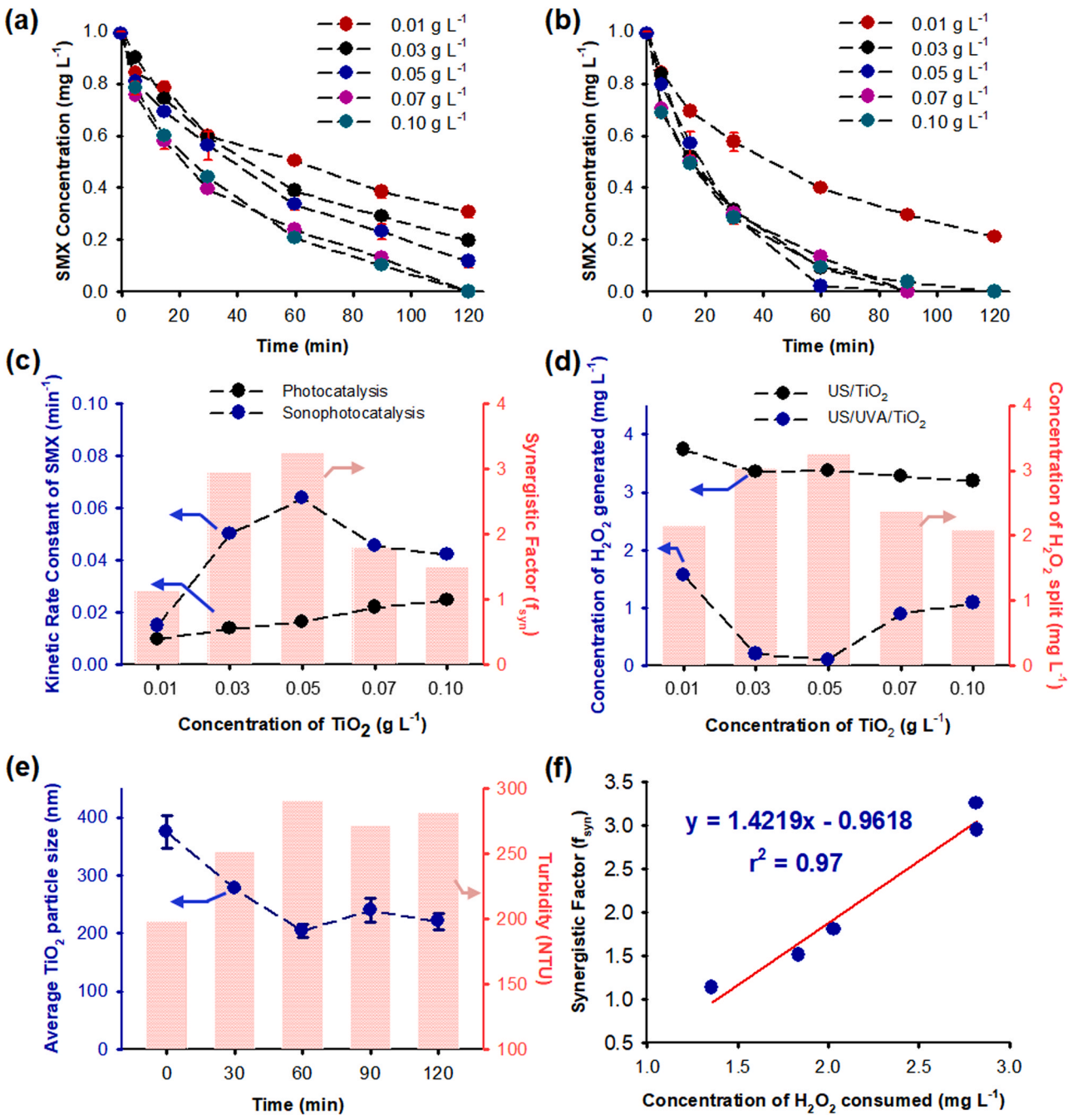

Fig. 5. Concentration effect of TiO_2 in SMX degradation under (a) photocatalysis, (b) sonophotocatalysis and (c) calculated kinetic rate constant. Concentration of H_2O_2 generated under US/TiO_2 and US/UVA/TiO_2 (d) and the consumption of H_2O_2 with different concentration of TiO_2. Kinetics of average particle size distribution of TiO_2 for 2 h of US irradiation (e) and followed by 2 h of stirring. A positive correlation between synergistic factor and concentration H_2O_2 split (f).

et al., 2019; Isari et al., 2020; Chen and Huang, 2011). Beyond doubt, this resulted in an unfavorable circumstance for TiO_2 activation. Turbidity changes after sole stirring or US irradiation were measured for various concentrations of TiO_2. As a result, the US irradiation gave a 118–151% increase (Fig. S18) in turbidity. In the case of 0.05 g L^{-1} of TiO_2, kinetic changes in the particle size distribution (PSD) and turbidity by US irradiation were found. The result [Fig. 5(e)] shows that the PSD of TiO_2 decreased significantly from 375.5 to 204.3 nm for 60 min and remained constant (~200 nm) until 120 min, whereas their turbidity increased. Therefore, along with this kinetic change in the PSD, relatively similar turbidity increases indicated that the de-agglomeration of TiO_2 for all dosages could be achieved equilibrium. Hence, by considering the de-agglomeration as a constant physical factor, the relationship between f_{syn} and the splitting of H_2O_2 concentration at each TiO_2 dosage was depicted in Fig. 5(f). Interestingly, there is a solid linear curve ($R^2 = 0.97$) was obtained, reflecting the interplay between the photoexcited e^- and H_2O_2 splitting governs the overall synergistic mechanism instead of de-agglomeration.

3.5. Sonophotocatalysis for treating municipal wastewater effluents

Based on our proposed mechanism, sonophotocatalysis condition should be able to generate sufficient concentrations of ROS in the gas-liquid interface and bulk liquid for effective degradation of both hydrophobic and hydrophilic POPs. The degradation of POPs in the MP wastewater treatment plant remained a challenge due to the high

contents of dissolved organic matter (DOM) with different physico-chemical properties. Most of the DOM could be indiscriminately oxidized by the generated ROS, leading to an unfavorable competition effect with POPs (Sheng et al., 2013; Pereira et al., 2013). As shown in Fig. 6(a)–(c), the degradation efficiencies of three selected POPs by sole photocatalysis were shown significantly decreased compared to DI water. In contrast, sonophotocatalysis achieved > 98% removal of these three POPs within 2 h even though their degradation rates slightly decreased as kinetic cycles increased. The degradation rates for BPA, ATZ, and SMX in MP wastewater [Fig. S19(a)–(b)] under photocatalysis were 1.3×10^{-2}, 1.4×10^{-2}, and 5.87×10^{-3} min^{-1}, respectively, while sonophotocatalysis had 3.4, 2.8 and 7.7 times higher degradation rates, i.e., 4.4×10^{-2}, 3.9×10^{-2} and 4.5×10^{-2} min^{-1} for BPA, ATZ, and SMX, accordingly. These results could be justified by the tremendous increase of ROS, especially the generation of ·OH. In Fig. S20(a), the US in sonophotocatalysis has a higher contribution ratio in MP wastewater than DI due to DOM's presence that significantly diminishes photocatalysis's degradation efficiency. This observation could provide insight on our proposed mechanism in this study, in which US provides a high concentration of H_2O_2 but requires assistance from photocatalytic activity to yield reactive ·OH. Note that the trends of POPs degradation dependency on US were similar in both MP wastewater and DI water [Fig. S20(b)]. Especially, the degradation of SMX was significantly dependent on the contribution of US in the MP wastewater matrix.

Unfortunately, the above results only imply the degradation of parent pollutants while the formation of by-products was not considered. Total organic carbon (TOC) contents were analyzed to determine the mineralization efficiencies between photocatalysis and sonophotocatalysis. For the initial MP wastewater, 17.5 mg L^{-1} of TOC was detected. After spiking with 0.1 mg L^{-1} of each POPs, the TOC concentration increased to 59.6 mg L^{-1}. Compared to the degradation results of parent POPs, the TOC was not effectively mineralized by photocatalysis [Fig. 6(d)], mainly owing to insufficient ROS generation. The mineralization rate of TOC in the 1st cycle was faster than those in the 2nd and 3rd cycles. Presumably, the ·OH oxidation reaction with organic matters to form carbon-centered radicals (·R or ·R-OH) and subsequently converted to organic peroxyl radicals (ROO·) in the presence of O_2. This ROO· further reacts to form reactive species such as H_2O_2 and $\cdot O_2^-$ simultaneously with the mineralization of the R-chain (Deng and Zhao, 2015). It should also be noted that the formed by-products could have different pK_a and K_{ow} values from the parent POPs. Since we have shown the sonophotocatalysis has the advantage of degrading various organic compounds due to the different regions created by US, the TOC concentration for all three cycles was effectively mineralized. Comparably, the photocatalytic degradation efficiency highly depending on the surface electrostatic interaction between the photocatalyst and organic compound (Jallouli et al., 2018).

3.6. Economic assessment for energy requirement

For practicability consideration, an economic assessment for energy requirement was conducted based on the mineralization of POPs and TOC in a unit volume (1 m^3) of POPs spiked into MP wastewater. The electric energy per order, E_{EO}, kWh m^{-3} was calculated according to the below equation (Eq. 4) (Azbar et al., 2004; Escudero et al., 2017):

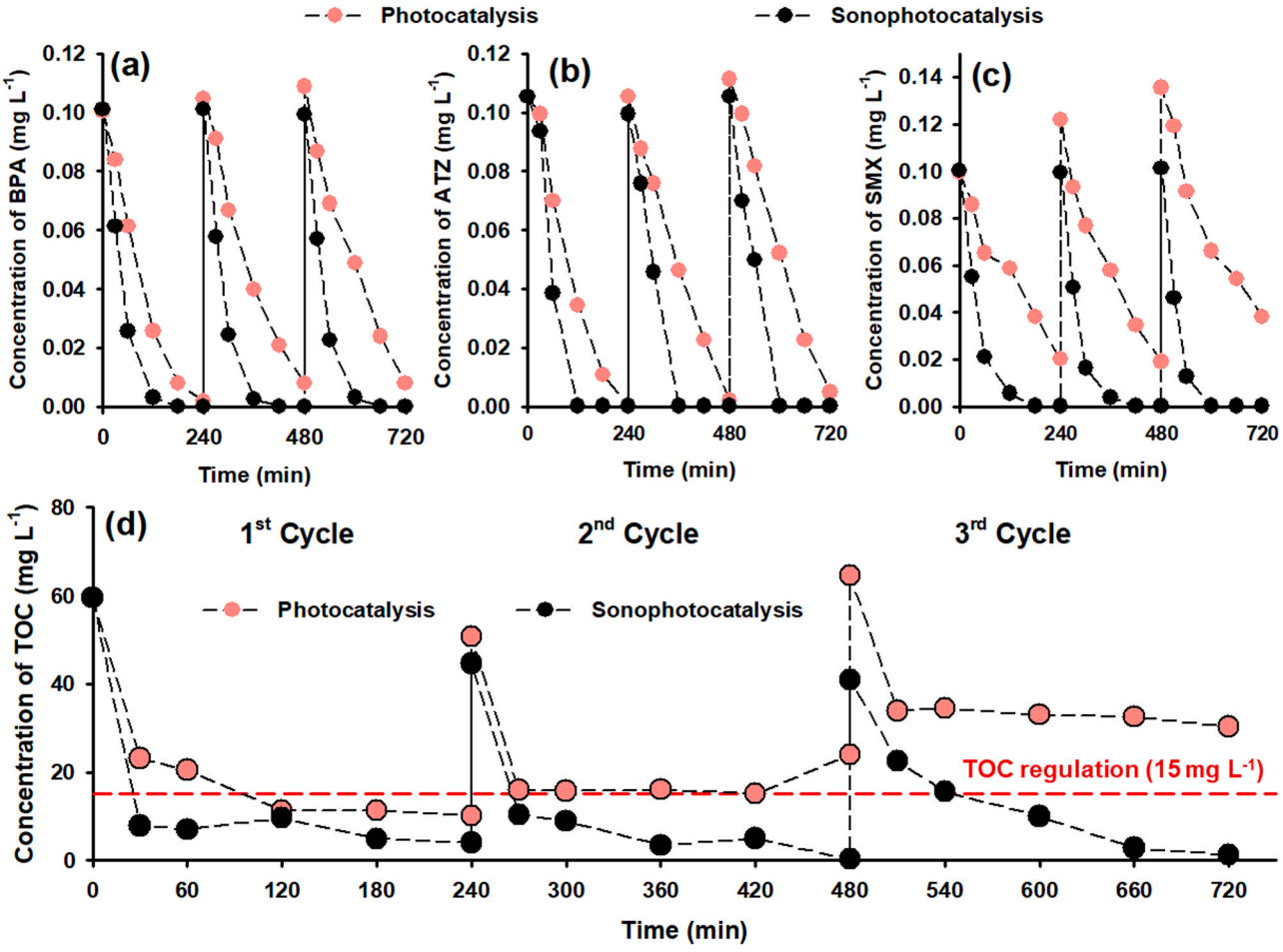

Fig. 6. Simultaneous degradation of (a) BPA, (b) ATZ and (c) SMX spiked into municipal wastewater for three consecutive cycles under photocatalysis and sonophotocatalysis and (d) mineralization efficiency of TOC. (* 0.1 mg L^{-1} of respective BPA, ATZ and SMX was spiked into the water matrices after each cycle).

$$E_{EO} = \frac{Pt \quad 1000}{\mathrm{Vlog}(C_0/C_t)} \tag{4}$$

where P is the total energy (kW) of sonophotocatalysis system (UVA: 8 W and US system: 50 W) and V is the volume of working solution (1 L) treated within t [2 h for POPs and 4 h for TOC; >96% of removed) while C_0 and C_t refer to the initial and final concentration (mg L^{-1}) of BPA, ATZ, SMX, and TOC, respectively. The E_{EO} of photocatalysis and sonophotocatalysis for POPs degradation was calculated and tabulated in Table S7.

Accordingly, these results show that sonophotocatalysis is more energy efficient in terms of mineralization rates than photocatalysis, which utilizes lower energy. Particularly SMX was shown to be recalcitrant towards photocatalysis as the E_{EO} was calculated to be 2–3 times higher than BPA and ATZ (Fig. S21). In contrast, the E_{EO} (3.0 kWh m^{-3}) for SMX degradation under sonophotocatalysis was 6.5 times lower than that under photocatalysis (19.6 kWh m^{-3}). To achieve > 96% mineralization of TOC, 8.1 and 26.7 kWh m^{-3} were required for photocatalysis and sonphotocatalysis, respectively.

Overall treatment energy costs were calculated according to (Eq. 5):

$$Treatmentenergycost\left(USDm^{-3}\right) = E_{EO-SPC} \times electricitycost \tag{5}$$

where $E_{EO\text{-}SPC}$ referred to E_{EO} of sonophotocatalysis. As of March 2020, the electricity price was USD 0.088 per kWh for the industry in South Korea. The estimated energy costs for 3 POPs and TOC in MP wastewater treatment were USD 0.24–0.26 and 0.72 m^{-3}. These energy costs were considerably cheaper compared to most studies (Table S8), especially for the mineralization of TOC.

4. Conclusions

Evidence from scavenging tests, H_2O_2 measurement, and ESR led us to an important conclusion where sonolysis and photocatalysis complemented each other through high selectivity for H_2O_2 splitting by the photoexcited e^- to produce a higher concentration of ROS, thereby increasing the ·OH concentration in the bulk liquid. This outcome is significant for the degradation of SMX as sonolytic cavitation produces a low concentration of ·OH in the bulk liquid. The integration of these two systems yielded a high synergistic factor (f_{syn}: 3.26) for the degradation of SMX. Whereas hydrophobic POPs have lower f_{syn}, i.e., BPA (K_{ow}: 3.32) and ATZ (K_{ow}: 2.61) had a value of 1.30 and 1.35, respectively are the resultant of BPA and ATZ degradation does not highly depend on the photoexcited e^- as the reaction primarily occurs at the gas-liquid interface. Furthermore, the interplay between photoexcited e^- and H_2O_2 splitting is shown linearly correlated with the f_{syn}, indicating that the sono-photochemical mechanism governs the overall synergism. Lastly, the economic assessment was estimated by calculating the E_{EO} (8.1 kWh m^{-3}) and electrical cost (USD 0.72 m^{-3}) based on TOC mineralization in actual MP wastewater effluent within 4 h. With average degradation percentage of POPs and TOC was >98 and >96% for the treatment duration of 2 and 4 h, respectively. We believe that this theoretical study advances the understanding of synergistic mechanisms and emphasizes the effective implications of sonophotocatalysis for the treatment of wastewater containing TOC and a broad spectrum of POPs.

CRediT authorship contribution statement

Baekha Ryu: Conceptualization, Methodology, Investigation, Writing - original draft, Writing - review & editing. **Kien Tiek Wong:** Conceptualization, Visualization, Investigation, Writing - original draft, Writing - review & editing. **Choe Earn Choong:** Writing - review & editing. **Jung-Rae Kim:** Resources, Validation. **Hyunook Kim:** Resources, Validation, Formal analysis. **Sang-Hyoun Kim:** Resources, Validation. **Byong-Hun Jeon:** Resources, Validation. **Yeomin Yoon:** Resources, Validation. **Shane A. Snyder:** Resources, Validation. **Min Jang:** Writing - original draft, Writing - review & editing, Supervision, Funding acquisition.

Declaration of Competing Interest

The authors declare that they have no known competing financial interests or personal relationships that could have appeared to influence the work reported in this paper.

Acknowledgment

The present research has been conducted by the Research Grant of Kwangwoon University in 2021, National Research Foundation, the Republic of Korea (No. 2020R1F1A1075839), and Korea Environment Industry & Technology Institute (Grant 2020002470002).

Appendix A. Supporting information

Supplementary data associated with this article can be found in the online version at doi:10.1016/j.jhazmat.2021.125787.

References

Adewuyi, Y.G., 2001. Sonochemistry: environmental science and engineering applications. Ind. Eng. Chem. Res. 40, 4681–4715.
Ahmedchekkat, F., Medjram, M.S., Chiha, M., Al-Bsoul, A.M.A., 2011. Sonophotocatalytic degradation of Rhodamine B using a novel reactor geometry: effect of operating conditions. Chem. Eng. J. 178, 244–251.
Ajo, P., Kornev, I., Preis, S., 2017. Pulsed corona discharge induced hydroxyl radical transfer through the gas-liquid interface. Sci. Rep. 7, 1–6.
Anju, S., Yesodharan, S., Yesodharan, E., 2012. Zinc oxide mediated sonophotocatalytic degradation of phenol in water. Chem. Eng. J. 189, 84–93.
Ayare, S.D., Gogate, P.R., 2020. Sonochemical, photocatalytic and sonophotocatalytic oxidation of flonicamid pesticide solution using different catalysts. Chem. Eng. Process. Process. Intensif. 154, 108040.
Azbar, N., Yonar, T., Kestioglu, K., 2004. Comparison of various advanced oxidation processes and chemical treatment methods for COD and color removal from a polyester and acetate fiber dyeing effluent. Chemosphere 55, 35–43.
Babu, S.G., Vinoth, R., Neppolian, B., Dionysiou, D.D., Ashokkumar, M., 2015. Diffused sunlight driven highly synergistic pathway for complete mineralization of organic contaminants using reduced graphene oxide supported photocatalyst. J. Hazard. Mater. 291, 83–92.
Bao, L.-J., Maruya, K.A., Snyder, S.A., Zeng, E.Y., 2012. China's water pollution by persistent organic pollutants. Environ. Pollut. 163, 100–108.
Brotchie, A., Grieser, F., Ashokkumar, M., 2009. Effect of power and frequency on bubble-size distributions in acoustic cavitation. Phys. Rev. Lett. 102, 084302.
Chen, W.-S., Huang, S.-C., 2011. Sonophotocatalytic degradation of dinitrotoluenes and trinitrotoluene in industrial wastewater. Chem. Eng. J. 172, 944–951.
Colmenares, J.C., Luque, R., 2014. Heterogeneous photocatalytic nanomaterials: prospects and challenges in selective transformations of biomass-derived compounds. Chem. Soc. Rev. 43, 765–778.
Cui, M., Choi, J., Lee, Y., Ma, J., Kim, D., Choi, J., Jang, M., Khim, J., 2017. Significant enhancement of bromate removal in drinking water: Implications for the mechanism of sonocatalytic reduction. Chem. Eng. J. 317, 404–412.
Deng, Y., Zhao, R., 2015. Advanced oxidation processes (AOPs) in wastewater treatment. Curr. Pollut. Rep. 1, 167–176.
Dharmarathne, L., Ashokkumar, M., Grieser, F., 2013. On the generation of the hydrated electron during the sonolysis of aqueous solutions. J. Phys. Chem. A 117, 2409–2414.
ElMetwally, A., Eshaq, G., Al-Sabagh, A., Yehia, F., Philip, C., Moussa, N., ElShafei, G.M., 2019. Insight into heterogeneous Fenton-sonophotocatalytic degradation of nitrobenzene using metal oxychlorides. Sep. Purif. Technol. 210, 452–462.
Escudero, C.J., Iglesias, O., Dominguez, S., Rivero, M.J., Ortiz, I., 2017. Performance of electrochemical oxidation and photocatalysis in terms of kinetics and energy consumption. New insights into the p-cresol degradation. J. Environ. Manag. 195, 117–124.
Eshaq, G., Wang, S., Sun, H., Sillanpaa, M., 2020. Superior performance of $FeVO_4$@ CeO_2 uniform core-shell nanostructures in heterogeneous Fenton-sonophotocatalytic degradation of 4-nitrophenol. J. Hazard. Mater. 382, 121059.
Fadzeelah, A.N., Abdullah, A., Zubir, N., Abd Razak, A., Azha, N., 2019. Sonocatalytic degradation of caffeine using CeO2 catalyst: parametric and reusability studies. J. Phys. Conf. Ser.
Gao, Y., Deshusses, M.A., 2011. Adsorption of clofibric acid and ketoprofen onto powdered activated carbon: effect of natural organic matter. Environ. Technol. 32, 1719–1727.
Goeury, K., Duy, S.V., Munoz, G., Prévost, M., Sauvé, S., 2019. Analysis of Environmental Protection Agency priority endocrine disruptor hormones and bisphenol A in tap, surface and wastewater by online concentration liquid chromatography tandem mass spectrometry. J. Chromatogr. A 1591, 87–98.

Gole, V.L., Priya, A., Danao, S.P., 2017. Decolorization of brilliant green dye using immersed lamp sonophotocatalytic reactor. Appl. Water Sci. 7, 4237–4245.
Granados-Oliveros, G., Páez-Mozo, E.A., Ortega, F.M., Ferronato, C., Chovelon, J.-M., 2009. Degradation of atrazine using metalloporphyrins supported on TiO_2 under visible light irradiation. Appl. Catal. B 89, 448–454.
Gupta, R., Modak, J., 2020. Bacterial lysis via photocatalysis-a critical mechanistic review. ChemCatChem 12, 2148–2170.
Hapeshi, E., Fotiou, I., Fatta-Kassinos, D., 2013. Sonophotocatalytic treatment of ofloxacin in secondary treated effluent and elucidation of its transformation products. Chem. Eng. J. 224, 96–105.
Henglein, A., 1995. Chemical effects of continuous and pulsed ultrasound in aqueous solutions. Ultrason. Sonochem. 2, S115–S121.
Henglein, A., Gutierrez, M., 1988. Sonolysis of polymers in aqueous solution. New observations on pyrolysis and mechanical degradation. Am. J. Phys. Chem. 92, 3705–3707.
Hoa, P.T.P., Managaki, S., Nakada, N., Takada, H., Shimizu, A., Anh, D.H., Viet, P.H., Suzuki, S., 2011. Antibiotic contamination and occurrence of antibiotic-resistant bacteria in aquatic environments of northern Vietnam. Sci. Total Environ. 409, 2894–2901.
Ince, N.H., Tezcanli-Güyer, G., 2004. Impacts of pH and molecular structure on ultrasonic degradation of azo dyes. Ultrasonics 42, 591–596.
Isari, A.A., Mehregan, M., Mehregan, S., Hayati, F., Kalantary, R.R., Kakavandi, B., 2020. Sono-photocatalytic degradation of tetracycline and pharmaceutical wastewater using WO_3/CNT heterojunction nanocomposite under US and visible light irradiations: a novel hybrid system. J. Hazard. Mater. 390, 122050.
Jagne, J., White, D., Jefferson, F., 2016. Endocrine-disrupting chemicals: adverse effects of bisphenol A and parabens to women's health. Water Air Soil Pollut. 227, 182.
Jallouli, N., Pastrana-Martínez, L.M., Ribeiro, A.R., Moreira, N.F., Faria, J.L., Hentati, O., Silva, A.M., Ksibi, M., 2018. Heterogeneous photocatalytic degradation of ibuprofen in ultrapure water, municipal and pharmaceutical industry wastewaters using a TiO2/UV-LED system. Chem. Eng. J. 334, 976–984.
Jinhua Ye, Gianluca, Li Puma, Jenny, Schneider, Detlef, Bahnemann, D.D., 2016. Dionysiou, Photocatalysis: Fundamentals and Perspectives. Royal Society of Chemistry.
Joseph, C.G., Puma, G.L., Bono, A., Krishnaiah, D., 2009. Sonophotocatalysis in advanced oxidation process: a short review. Ultrason. Sonochem. 16, 583–589.
Jun, B.-M., Kim, S., Heo, J., Her, N., Jang, M., Park, C.M., Yoon, Y., 2019. Enhanced sonocatalytic degradation of carbamazepine and salicylic acid using a metal-organic framework. Ultrason. Sonochem. 56, 174–182.
Kakavandi, B., Bahari, N., Kalantary, R.R., Fard, E.D., 2019. Enhanced sono-photocatalysis of tetracycline antibiotic using TiO_2 decorated on magnetic activated carbon (MAC@T) coupled with US and UV: a new hybrid system. Ultrason. Sonochem. 55, 75–85.
Katsoyiannis, A., Samara, C., 2005. Persistent organic pollutants (POPs) in the conventional activated sludge treatment process: fate and mass balance. Environ. Res. 97, 245–257.
Khataee, A., Fathinia, M., 2013. Recent Advances in Photocatalytic Processes by Nanomaterials, New and Future Developments in Catalysis. Elsevier, pp. 267–288.
Kormann, C., Bahnemann, D.W., Hoffmann, M.R., 1988. Photocatalytic production of hydrogen peroxides and organic peroxides in aqueous suspensions of titanium dioxide, zinc oxide, and desert sand. Environ. Sci. Technol. 22, 798–806.
Lee, G., Ibrahim, S., Kittappa, S., Park, H., Park, C.M., 2018. Sonocatalytic activity of a heterostructured β-Bi2O3/Bi2O2CO3 nanoplate in degradation of bisphenol A. Ultrason. Sonochem. 44, 64–72.
Liu, B., Wang, X., Wen, L., Zhao, X., 2013. Investigation of electron behavior in nano-tio2 photocatalysis by using in situ open-circuit voltage and photoconductivity measurements. Chem. Eur. J. 19, 10751–10759.
Madhavan, J., Kumar, P.S.S., Anandan, S., Grieser, F., Ashokkumar, M., 2010. Degradation of acid red 88 by the combination of sonolysis and photocatalysis. Sep. Purif. Technol. 74, 336–341.
Mailloux, R.J., 2015. Teaching the fundamentals of electron transfer reactions in mitochondria and the production and detection of reactive oxygen species. Redox Biol. 4, 381–398.
Mehrizad, A., Behnajady, M.A., Gharbani, P., Sabbagh, S., 2019. Sonocatalytic degradation of Acid Red 1 by sonochemically synthesized zinc sulfide-titanium dioxide nanotubes: optimization, kinetics and thermodynamics studies. J. Clean. Prod. 215, 1341–1350.
Méndez-Arriaga, F., Torres-Palma, R., Pétrier, C., Esplugas, S., Gimenez, J., Pulgarin, C., 2008. Ultrasonic treatment of water contaminated with ibuprofen. Water Res. 42, 4243–4248.
Merouani, S., Hamdaoui, O., Boutamine, Z., Rezgui, Y., Guemini, M., 2016. Experimental and numerical investigation of the effect of liquid temperature on the sonolytic degradation of some organic dyes in water. Ultrason. Sonochem. 28, 382–392.
Michael, I., Achilleos, A., Lambropoulou, D., Torrens, V.O., Pérez, S., Petrović, M., Barceló, D., Fatta-Kassinos, D., 2014. Proposed transformation pathway and evolution profile of diclofenac and ibuprofen transformation products during (sono) photocatalysis. Appl. Catal. B Environ. 147, 1015–1027.
Monteagudo, J., Durán, A., San Martín, I., García, S., 2014. Ultrasound-assisted homogeneous photocatalytic degradation of Reactive Blue 4 in aqueous solution. Appl. Catal. B 152, 59–67.
Mosleh, S., Rahimi, M.R., 2017. Intensification of abamectin pesticide degradation using the combination of ultrasonic cavitation and visible-light driven photocatalytic process: synergistic effect and optimization study. Ultrason. Sonochem. 35, 449–457.
Mullick, A., Neogi, S., 2017. A review on acoustic methods of algal growth control by ultrasonication through existing and novel emerging technologies. Rev. Chem. Eng. 33, 469–490.
Naddeo, V., Belgiorno, V., Kassinos, D., Mantzavinos, D., Meric, S., 2010. Ultrasonic degradation, mineralization and detoxification of diclofenac in water: optimization of operating parameters. Ultrason. Sonochem. 17, 179–185.
Nuengmatcha, P., Chanthai, S., Mahachai, R., Oh, W.-C., 2016. Sonocatalytic performance of ZnO/graphene/TiO2 nanocomposite for degradation of dye pollutants (methylene blue, texbrite BAC-L, texbrite BBU-L and texbrite NFW-L) under ultrasonic irradiation. Dyes Pigment. 134, 487–497.
Paleologou, A., Marakas, H., Xekoukoulotakis, N.P., Moya, A., Vergara, Y., Kalogerakis, N., Gikas, P., Mantzavinos, D., 2007. Disinfection of water and wastewater by TiO_2 photocatalysis, sonolysis and UV-C irradiation. Catal. Today 129, 136–142.
Peller, J., Wiest, O., Kamat, P.V., 2003. Synergy of combining sonolysis and photocatalysis in the degradation and mineralization of chlorinated aromatic compounds. Environ. Sci. Tech. 37, 1926–1932.
Pereira, J.H., Reis, A.C., Queirós, D., Nunes, O.C., Borges, M.T., Vilar, V.J., Boaventura, R.A., 2013. Insights into solar TiO2-assisted photocatalytic oxidation of two antibiotics employed in aquatic animal production, oxolinic acid and oxytetracycline. Sci. Total Environ. 463, 274–283.
Pokhrel, N., Vabbina, P.K., Pala, N., 2016. Sonochemistry: science and engineering. Ultrason. Sonochem. 29, 104–128.
Rad, T.S., Ansarian, Z., Soltani, R.D.C., Khataee, A., Orooji, Y., Vafaei, F., 2020. Sonophotocatalytic activities of FeCuMg and CrCuMg LDHs: Influencing factors, antibacterial effects, and intermediate determination. J. Hazard. Mater. 399, 123062.
Saien, J., Delavari, H., Solymani, A., 2010. Sono-assisted photocatalytic degradation of styrene-acrylic acid copolymer in aqueous media with nano titania particles and kinetic studies. J. Hazard. Mater. 177, 1031–1038.
Sancheti, S.V., Saini, C., Ambati, R., Gogate, P.R., 2018. Synthesis of ultrasound assisted nanostuctured photocatalyst (NiO supported over CeO2) and its application for photocatalytic as well as sonocatalytic dye degradation. Catal. Today 300, 50–57.
Savun-Hekimoğlu, B., Ince, N.H., 2017. Decomposition of PPCPs by ultrasound-assisted advanced Fenton reaction: a case study with salicylic acid. Ultrason. Sonochem. 39, 243–249.
Savun-Hekimoğlu, B., Ince, N.H., 2019. Sonochemical and sonocatalytic destruction of methylparaben using raw, modified and SDS-intercalated particles of a natural clay mineral. Ultrason. Sonochem. 54, 233–240.
Selim, A., Kaur, S., Dar, A.H., Sartaliya, S., Jayamurugan, G., 2020. Synergistic effects of carbon dots and palladium nanoparticles enhance the sonocatalytic performance for rhodamine B degradation in the absence of light. ACS Omega 5, 22603–22613.
Shende, T., Andaluri, G., Suri, R.P., 2019. Kinetic model for sonolytic degradation of non-volatile surfactants: perfluoroalkyl substances. Ultrason. Sonochem. 51, 359–368.
Sheng, H., Li, Q., Ma, W., Ji, H., Chen, C., Zhao, J., 2013. Photocatalytic degradation of organic pollutants on surface anionized TiO_2: common effect of anions for high hole-availability by water. Appl. Catal. B Environ. 138, 212–218.
Singh, S., Kumar, V., Chauhan, A., Datta, S., Wani, A.B., Singh, N., Singh, J., 2018. Toxicity, degradation and analysis of the herbicide atrazine. Environ. Chem. Lett. 16, 211–237.
Soltani, R.D.C., Safari, M., Mashayekhi, M., 2016. Sonocatalyzed decolorization of synthetic textile wastewater using sonochemically synthesized MgO nanostructures. Ultrason. Sonochem. 30, 123–131.
Stackelberg, P.E., Furlong, E.T., Meyer, M.T., Zaugg, S.D., Henderson, A.K., Reissman, D. B., 2004. Persistence of pharmaceutical compounds and other organic wastewater contaminants in a conventional drinking-water-treatment plant. Sci. Total Environ. 329, 99–113.
Tabasideh, S., Maleki, A., Shahmoradi, B., Ghahremani, E., McKay, G., 2017. Sonophotocatalytic degradation of diazinon in aqueous solution using iron-doped TiO2 nanoparticles. Sep. Purif. Technol. 189, 186–192.
Torres, R.A., Nieto, J.I., Combet, E., Pétrier, C., Pulgarin, C., 2008. Influence of TiO_2 concentration on the synergistic effect between photocatalysis and high-frequency ultrasound for organic pollutant mineralization in water. Appl. Catal. B 80, 168–175.
Torres, R.A., Pétrier, C., Combet, E., Carrier, M., Pulgarin, C., 2008. Ultrasonic cavitation applied to the treatment of bisphenol A. Effect of sonochemical parameters and analysis of BPA by-products. Ultrason. Sonochem. 15, 605–611.
Wang, X., Wang, J., Guo, P., Guo, W., Wang, C., 2009. Degradation of rhodamine B in aqueous solution by using swirling jet-induced cavitation combined with H_2O_2. J. Hazard. Mater. 169, 486–491.
Wong, K.T., Kim, S.C., Yun, K., Choong, C.E., Nah, I.W., Jeon, B.-H., Yoon, Y., Jang, M., 2020. Understanding the potential band position and e^-/h^+ separation lifetime for Z-scheme and type-II heterojunction mechanisms for effective micropollutant mineralization: Comparative experimental and DFT studies. Appl. Catal. B Environ. 273, 119034.
Wood, R.J., Lee, J., Bussemaker, M.J., 2017. A parametric review of sonochemistry: control and augmentation of sonochemical activity in aqueous solutions. Ultrason. Sonochem. 38, 351–370.
Wu, Z., Ondruschka, B., 2005. Roles of hydrophobicity and volatility of organic substrates on sonolytic kinetics in aqueous solutions. J. Phys. Chem. A 109, 6521–6526.
Xu, H., Zeiger, B.W., Suslick, K.S., 2013. Sonochemical synthesis of nanomaterials. Chem. Soc. Rev. 42, 2555–2567.
Yasui, K., Tuziuti, T., Lee, J., Kozuka, T., Towata, A., Iida, Y., 2008. The range of ambient radius for an active bubble in sonoluminescence and sonochemical reactions. J. Chem. Phys. 128, 184705.

Zargazi, M., Entezari, M.H., 2019. Sonochemical versus hydrothermal synthesis of bismuth tungstate nanostructures: photocatalytic, sonocatalytic and sonophotocatalytic activities. Ultrason. Sonochem. 51, 1–11.

Zhou, P., Yu, J., Jaroniec, M., 2014. All-solid-state Z-scheme photocatalytic systems. Adv. Mater. 26, 4920–4935.

Zuccato, E., Calamari, D., Natangelo, M., Fanelli, R., 2000. Presence of therapeutic drugs in the environment. Lancet 355, 1789–1790.